

University of Groningen

## Understanding the Surface Chemistry of SnO<sub>2</sub> Nanoparticles for High Performance and Stable Organic Solar Cells

Garcia Romero, David; Di Mario, Lorenzo; Yan, Feng; Ibarra-Barreno, Carolina Mishell; Mutalik, Suhas; Protesescu, Loredana; Rudolf, Petra; Loi, Maria Antonietta

*Published in:*  
Advanced Functional Materials

*DOI:*  
[10.1002/adfm.202307958](https://doi.org/10.1002/adfm.202307958)

**IMPORTANT NOTE: You are advised to consult the publisher's version (publisher's PDF) if you wish to cite from it. Please check the document version below.**

*Document Version*  
Version created as part of publication process; publisher's layout; not normally made publicly available

*Publication date:*  
2023

[Link to publication in University of Groningen/UMCG research database](#)

*Citation for published version (APA):*

Garcia Romero, D., Di Mario, L., Yan, F., Ibarra-Barreno, C. M., Mutalik, S., Protesescu, L., Rudolf, P., & Loi, M. A. (in press). Understanding the Surface Chemistry of SnO<sub>2</sub> Nanoparticles for High Performance and Stable Organic Solar Cells. *Advanced Functional Materials*, Article 2307958. <https://doi.org/10.1002/adfm.202307958>

### Copyright

Other than for strictly personal use, it is not permitted to download or to forward/distribute the text or part of it without the consent of the author(s) and/or copyright holder(s), unless the work is under an open content license (like Creative Commons).

The publication may also be distributed here under the terms of Article 25fa of the Dutch Copyright Act, indicated by the "Taverne" license. More information can be found on the University of Groningen website: <https://www.rug.nl/library/open-access/self-archiving-pure/taverne-amendment>.

### Take-down policy

If you believe that this document breaches copyright please contact us providing details, and we will remove access to the work immediately and investigate your claim.

Downloaded from the University of Groningen/UMCG research database (Pure): <http://www.rug.nl/research/portal>. For technical reasons the number of authors shown on this cover page is limited to 10 maximum.

# Understanding the Surface Chemistry of SnO<sub>2</sub> Nanoparticles for High Performance and Stable Organic Solar Cells

David Garcia Romero, Lorenzo Di Mario, Feng Yan, Carolina Mishell Ibarra-Barreno, Suhas Mutalik, Loredana Protesescu, Petra Rudolf, and Maria Antonietta Loi\*

In organic solar cells, the interfaces between the photoactive layer and the transport layers are critical in determining not only the efficiency but also their stability. When solution-processed metal oxides are employed as the electron transport layer, the presence of surface defects can downgrade the charge extraction, lowering the photovoltaic parameters. Thus, understanding the origin of these defects is essential to prevent their detrimental effects. Herein, it is shown that a widely reported and commercially available colloidal SnO<sub>2</sub> dispersion leads to suboptimal interfaces with the organic layer, as evidenced by the s-shaped *J*-*V* curves and poor stability. By investigating the SnO<sub>2</sub> surface chemistry, the presence of potassium ions as stabilizing ligands is identified. By removing them with a simple washing with deionized water, the s-shape is removed and the short-circuit current is improved. It is tested for two prototypical blends, TPD-3F:IT-4F and PM6:L8:BO, and for both the power conversion efficiency is improved up to 12.82% and 16.26%, from 11.06% and 15.17% obtained with the pristine SnO<sub>2</sub>, respectively. More strikingly, the stability is strongly correlated with the surface ions concentration, and these improved devices maintain  $\approx 87\%$  and  $\approx 85\%$  of their initial efficiency after 100 h of illumination for TPD-3F:IT-4F and PM6:L8:BO, respectively.

molecules, which can take advantage of increased light absorption and form finer morphologies, still capture most of the attention in lab-scale devices.<sup>[3]</sup> Nevertheless, for a transition from lab-based solar cell fabrication to mass production, it is imperative to develop optimal interlayers, which can benefit from scalable and low-cost processing. Currently, sol-gel ZnO is predominantly chosen as the cathode interlayer for best-performing n-i-p solar cells.<sup>[2,4-6]</sup> Nevertheless, this method requires high annealing temperatures and is very sensitive to small variations in the processing conditions, posing reproducibility problems.<sup>[7,8]</sup> Moreover, ZnO has been reported to trigger photodegradation of photoactive molecules at the interface, thus strongly affecting device stability.<sup>[9,10]</sup> Recently, SnO<sub>2</sub> has emerged as an alternative to ZnO due to its proven high electron mobility of over 400 cm<sup>2</sup> V s<sup>-1</sup> and wider bandgap, making it less sensitive to UV light.<sup>[11-13]</sup> Its deposition from a colloidal


## 1. Introduction

Bulk-heterojunction organic solar cells have experienced an extraordinary upsurge in performance within the last decade, fervently approaching 20% power conversion efficiency.<sup>[1,2]</sup> Nowadays, the development of new photoactive polymers and small

dispersion of nanoparticles in nontoxic solvents like ethanol or water has become a standard, especially in the field of perovskite solar cells.<sup>[11,14,15]</sup> In particular, the commercially available Alfa Aesar water-based SnO<sub>2</sub> (Alfa-SnO<sub>2</sub>) is one of the most promising options due to its low cost and benign solvent, making it an excellent candidate for a lab-to-fab transition.<sup>[16-18]</sup> Unfortunately, surface defects are inherent to nanoparticle surfaces, which ultimately can affect negatively the interface with the active layer, and the device performance.<sup>[19]</sup> Intriguingly, while several groups have reported passivation methods for the SnO<sub>2</sub> nanoparticle surface that employ for instance organic molecules,<sup>[20-23]</sup> quantum dots,<sup>[24]</sup> or even perovskite nanowires,<sup>[25]</sup> an accurate description of the origin of the surface defects is still missing. Moreover, these reported treatments usually involve complex procedures that are hard to reproduce and mostly incompatible with industrial processes.

Herein, we elucidate the fundamental reason why the widely used Alfa-SnO<sub>2</sub> forms a defective interface in organic solar cells. We prove that potassium ions, which are employed to obtain colloidal stability in water, remain electrostatically bonded on the surface of the thin films. This ionic coverage limits

D. Garcia Romero, L. Di Mario, F. Yan, C. M. Ibarra-Barreno, S. Mutalik, L. Protesescu, P. Rudolf, M. A. Loi  
Zernike Institute for Advanced Materials  
University of Groningen  
Nijenborgh 4, Groningen 9747 AG, The Netherlands  
E-mail: m.a.loi@rug.nl

 The ORCID identification number(s) for the author(s) of this article can be found under <https://doi.org/10.1002/adfm.202307958>

© 2023 The Authors. Advanced Functional Materials published by Wiley-VCH GmbH. This is an open access article under the terms of the Creative Commons Attribution License, which permits use, distribution and reproduction in any medium, provided the original work is properly cited.

DOI: 10.1002/adfm.202307958

electron extraction in the solar cells, leads to s-shaped  $J-V$  curves, and causes modest performance and poor device stability. By using a very simple water-based washing method to remove the potassium, we mitigate the light soaking and increase the efficiency of our solar cells without the need for any further passivation or treatment. In particular, we prove this for two different blends, one composed of the polymer poly[2,2'-(4,8-bis[4-fluoro-5-(2-hexyldecyl)-2-thienyl]benzo[1,2-b:4,5-b']dithiophene-2,6-diyl)-2,5-thiophenediyl(5,6-dihydro-5-octyl-4,6-dioxo-4H-thieno[3,4-c]pyrrole-1,3-diyl)-2,5-thiophenediyl] (TPD-3F) and the small molecule 3,9-bis(2-methylene-(3-(1,1-dicyanomethylene)-6,7-difluoro)-indanone)-5,5,11,11-tetrakis(4-hexylphenyl)-dithieno[2,3-d:2',3'-d']s-indaceno[1,2-b:5,6-b']dithiophene (IT-4F), and another one composed of the polymer Poly[(2,6-(4,8-bis(5-(2-ethylhexyl-3-fluoro)thiophen-2-yl)-benzo[1,2-b:4,5-b']dithiophene))-alt-(5,5-(1',3'-di-2-thienyl-5',7'-bis(2-ethylhexyl)benzo[1',2'-c:4',5'-c']dithiophene-4,8-dione)] (PM6) and small molecule 2,2'-((2Z,2'Z)-((12,13-bis(2-ethylhexyl)-3,9-(2-butyl)octyl)-12,13-dihydro-[1,2,5]thiadiazolo[3,4-e]thieno[2'',3'':4',5']thieno[2',3':4,5]pyrrolo[3,2-g]thieno[2',3':4,5]thieno[3,2-b]indole-2,10-diyl)bis(methanylylidene))bis(5,6-difluoro-3-oxo-2,3-dihydro-1H-indene-2,1-diylidene))dimalononitrile (L8-BO). The efficiencies of the corresponding devices increased with the treatment from 11.06% to 12.82% and from 15.17% to 16.26%, respectively. More strikingly, we found that the operational stability under illumination is strongly correlated with the concentration of surface ions, and their elimination promoted a device efficiency of  $\approx 87\%$  and  $\approx 85\%$  of the starting value after 100 h of continuous illumination for TPD-3F:IT-4F and PM6:L8:BO, respectively. Finally, by bringing back potassium on the washed  $\text{SnO}_2$  surfaces we could further confirm that the ions are responsible for the defective interface. Our work represents a substantial leap forward in the universal use of low-cost and scalable  $\text{SnO}_2$  electron transport layers for organic solar cells.

## 2. Results and Discussion

To illustrate the suboptimal interface between  $\text{SnO}_2$  and the organic active layers, we fabricated solar cells with an n-i-p structure of ITO/Alfa- $\text{SnO}_2$ /Active layer/ $\text{MoO}_x$ /Al (Figure 1a). Two different blend combinations, namely TPD-3F:IT-4F and PM6:L8-BO, were selected due to their outstanding performance reported previously<sup>[10,26]</sup> (Figure 1b). More details about the fabrication process can be found in the Experimental Section. The  $J-V$  characteristics of the solar cells are displayed in Figure 1c; here, an obvious s-shaped current output in the first measurement can be observed, and only after  $\approx 15$  min of light soaking the  $J-V$  curves for both blends recover their ideal shape. This phenomenon is well reported in the literature and has been explained by the formation of sub-gap trap states at the interface between the metal-oxide layer and the active layer. These states cause band bending at the interface and ultimately prevent an effective electron extraction. The improvement in charge extraction with illumination time has been explained by either de-trapping<sup>[27,28]</sup> or trap filling.<sup>[29]</sup> The evaluation of the dark current after different light soaking times was used to estimate the ideality factor and series resistance values with illumination time (Figure S1, Supporting Information). The improvement in the diode parameters over time is in agreement with the increased conductivity at the in-

terface and with the positive evolution of the fill factor. Overall, these results disclose a possible reason why Alfa- $\text{SnO}_2$  has not yet become a benchmark electron transport material in organic solar cells, and explain why many groups reported on the need for often complex and hazardous surface passivation strategies to obtain well-performing cells (Table S1, Supporting Information).

To determine the origin of the suboptimal interface, we started by characterizing the  $\text{SnO}_2$  nanoparticles from the colloidal dispersion by dynamic light scattering (DLS) and zeta-potential measurements (Figure S2, Supporting Information). The nanoparticles have a size of 13.6 nm with a narrow size distribution, and with a small aggregation as deduced from the broadening at larger sizes. A zeta potential of  $-34.16$  mV shows that deprotonated functional groups are present in the nanoparticle ligands.<sup>[30]</sup> This correlates well with the suspension's measured high basicity (pH 11) and points towards the presence of positive counterions, which can assist the colloidal stability in water.<sup>[31]</sup> This pH value is obtained even after the particles were left to precipitate and were subsequently re-dispersed in water several times, implying that the ligands are strongly attached to the surface of the NPs and they are responsible for the alkaline character. Conversely, when the nanoparticles were left to precipitate and were re-dispersed in methanol, the solution became unstable, showing that the ligands are highly sensitive to small changes in solvent polarity (Figure S2c, Supporting Information).

To enlighten the nature of the ligands, X-ray photoelectron spectroscopy (XPS) was performed on  $\text{SnO}_2$  films spin-coated on an ITO substrate (Figure 2a,b). The relative atomic concentration of the surface is shown in Table S2 (Supporting Information). A carbon concentration of 14.7 at% was calculated, revealing that a considerable amount of organic ligands is still present on the thin film surface, even after annealing. Surprisingly, a prominent  $\text{K}2p$  signal was observed, corresponding to a potassium concentration of 9.6 at%.

Based on the XPS measurements, it is reasonable to hypothesize that the residual species on the film surface could affect the interfacial properties. In particular, the low ionization energy of potassium is expected to determine the electrical character and reactivity of the interface. Therefore, we decided to remove potassium from the  $\text{SnO}_2$  surface: after depositing and annealing a  $\text{SnO}_2$  film, we performed a washing step with deionized water (DI-wash) followed by drying the film in the air at  $100^\circ\text{C}$  (Figure 2c). As can be observed in the XPS spectra (Figure 2b) and Table S2 (Supporting Information), potassium is fully eliminated from the surface through this simple process. Second, the binding energies of the tin and oxygen remain unaffected, which indicates that we do not significantly modify their chemical environment with surface washing (Figure S3, Supporting Information). Finally, the relative atomic concentration of carbon atom with respect to tin does not change, suggesting that the DI-washing is not capable of removing the ligands, and it has a unique effect on the potassium counter-ions.

To further investigate the surface composition, Fourier transform infrared (FTIR) spectra of the  $\text{SnO}_2$  thin films were collected before and after washing with DI-water (Figure 2d). The absorption peaks in the region  $1600\text{--}1300\text{ cm}^{-1}$  can be assigned to carboxylate bands.<sup>[32]</sup> The use of carboxylate salts to improve the water dispersibility of nanoparticles is a commonly used strategy.<sup>[30,33]</sup> The location and separation between the peaks

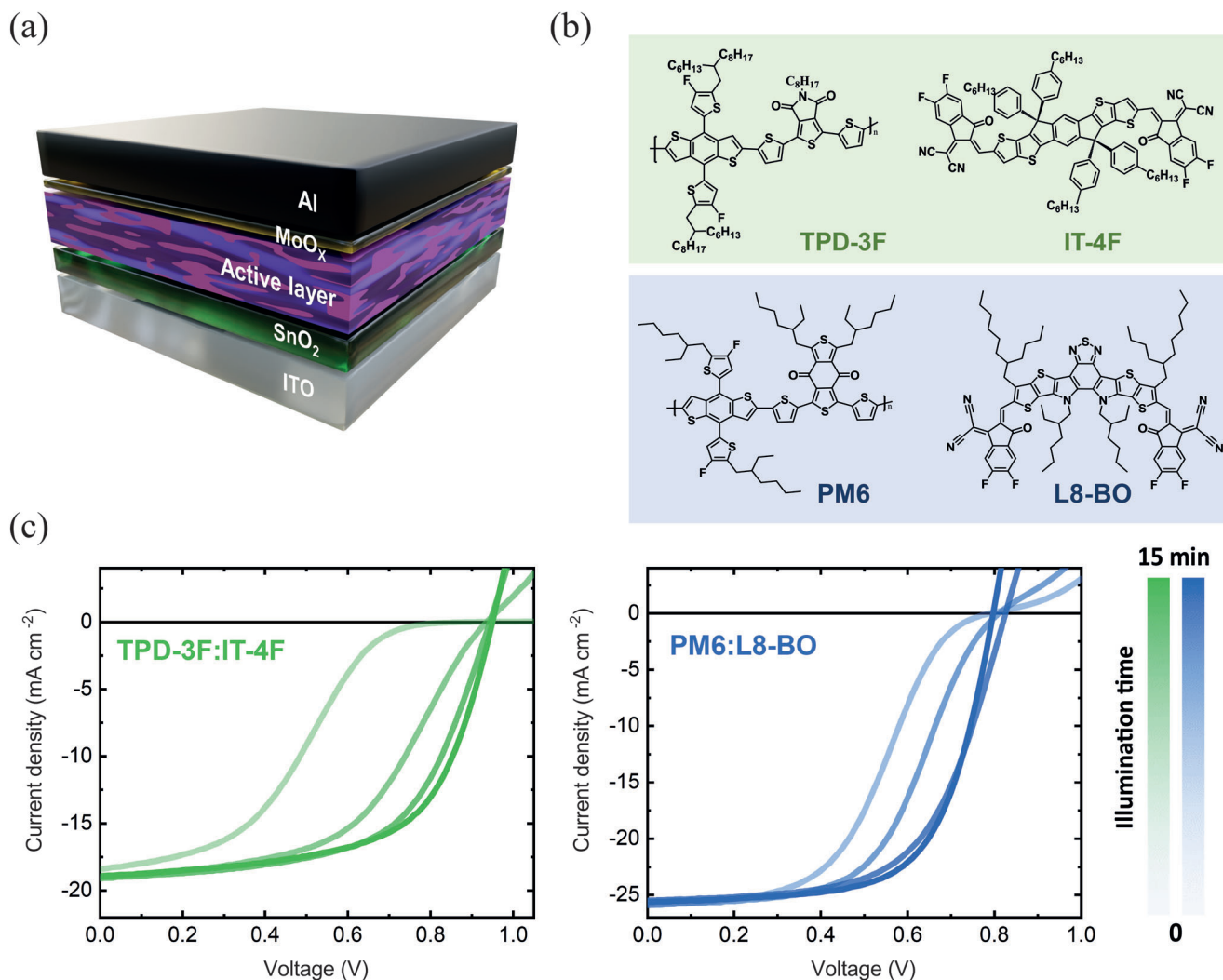


**Figure 1.** Organic solar cells with pristine Alfa-SnO<sub>2</sub> nanoparticles. a) Device structure used in this work; b) chemical structure of the two polymers and the small molecules employed; c) *J*-*V* characteristics of the two types of solar cells as a function of light soaking time.

inform about the carboxylate coordination mode; the bands at 1485 and 1332 cm<sup>-1</sup> correspond to bidentate coordination (–COO<sup>-</sup>), while the peak at 1638 cm<sup>-1</sup> corresponds to the C=O stretching of the acidic form (–COOH).<sup>[32]</sup> After washing most of the carboxylate ion becomes carboxylic acid, suggesting a hydroxylation of the negative oxygen atom upon the potassium removal from the film surface (Figure 2e). In brief, potassium cations that stabilize the negatively charged carboxylate end groups of the nanoparticles, stay bonded when the NPs are processed into thin films and are effectively removed by washing, in agreement with the XPS observations.

We used atomic force microscopy to assess whether the washing step had an impact on the SnO<sub>2</sub> film roughness. The film showed an RMS roughness of 1.501 ± 0.172 and 1.578 ± 0.158 nm (Figure S4, Supporting Information) before and after washing, respectively. Hence, washing does not have any impact on the surface topography of SnO<sub>2</sub>. It has a marginal effect on the thickness of the SnO<sub>2</sub> layers, which shows a decrease from 24.6 to 23.4 nm with the washing, as assessed by ellipsome-

try measurements. We believe that this slight drop might be due to the removal of unbounded residual ligands.

To demonstrate that the potassium ions on the SnO<sub>2</sub> surface have a detrimental effect, we fabricated solar cells comparing pristine SnO<sub>2</sub> and SnO<sub>2</sub> washed with DI-water as cathode interlayers, using the same organic blends shown earlier. The *J*-*V* characteristics of the cells, power conversion efficiencies (PCE), and external quantum efficiencies (EQE) are displayed in Figure 3, where the last measurement for the pristine SnO<sub>2</sub> was taken after the sample recovered from the s-shape with 15 min of light soaking. First, the DI-washing removed completely the s-shape issue, and ideal *J*-*V* curves were observed immediately upon illumination. Furthermore, the washing had a positive effect on the photovoltaic parameters, in particular on the short-circuit current (Table 1). This led to a systematic increase in the power conversion efficiencies, with an improvement of the efficiency of the record devices from 11.06% to 12.82% and from 15.17% to 16.26% for the TPD-3F:IT-4F and PM6:L8-BO blends, respectively. To the best of our knowledge, these values



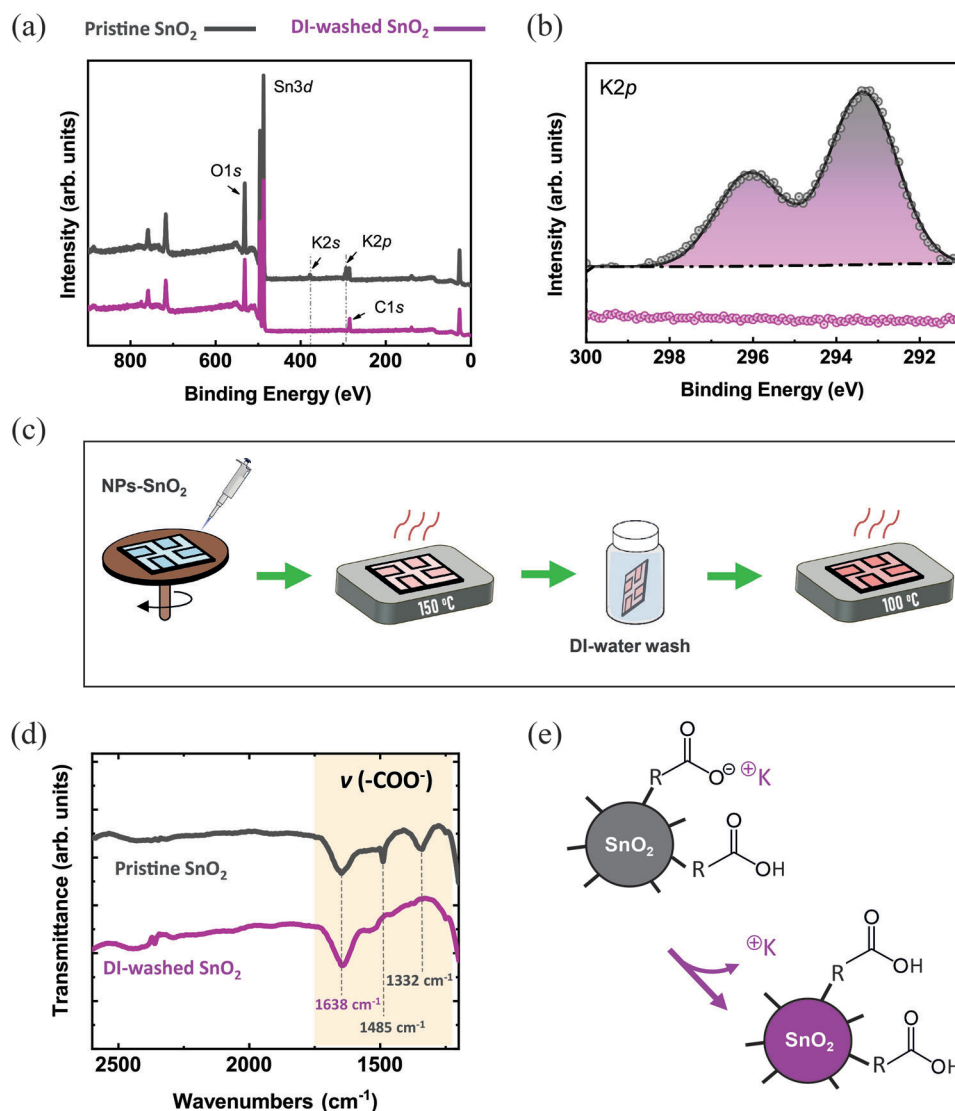


**Figure 2.** Surface chemistry of  $\text{SnO}_2$  films. a, b) XPS spectra of  $\text{SnO}_2$  films before and after washing with DI-water a) wide survey scan and b)  $\text{K}2p$  core level region; c) schematics of the deposition of  $\text{SnO}_2$  nanoparticles on the substrate and the washing process with DI-water; d) FTIR transmittance spectra the carboxylate bands absorption region of the  $\text{SnO}_2$  thin films before and after washing with DI-water; e) proposed mechanism for potassium removal upon washing with DI-water.

are among the highest within the reported PCEs for organic solar cells with  $\text{SnO}_2$  nanoparticles as an electron transport layer (Table S3, Supporting Information). The improved efficiency was also accompanied by higher reproducibility and a reduced standard deviation (insets Figure 3a,c). The increased short-circuit current was also evidenced by an improved external quantum efficiency (EQE).

Impedance spectroscopy is a useful tool to better understand the role of interfaces in charge recombination in solar cells.<sup>[34]</sup> Figure 4a shows the Nyquist plot, measured on the same device structure with the TPD-3F:IT-4F blend, in dark and at open circuit bias conditions, together with the best fitting curves. Under these conditions, the recombination of injected charges is maximized and there is an absence of photogenerated carriers. The equivalent electric circuits used for the fitting curves with the

extracted parameters are shown in Table S4 (Supporting Information). First, the series resistance of the main R-RC element decreased from 105 to 62.18  $\Omega$  with washing, implying that electrons are more easily transferred at the interface of the washed samples. Considering that the anode interface is the same for both samples, the difference can be assigned only to the differences within the  $\text{SnO}_2$ /blend interface. Second, the DI-washing decreased the parallel resistance from 1674 to 782.9  $\Omega$ . Generally, a higher parallel resistance is thought to indicate a better interface due to lower recombination.<sup>[35]</sup> However, it is important to note that the total parallel resistance is ultimately affected by the effective charge injection and therefore, what needs to be compared is the charge lifetime from the RC factors. An increase from 0.062 to 0.242  $\mu\text{s}$  indicates that washing decreased surface recombination. Interestingly, a second relaxation process was observed at

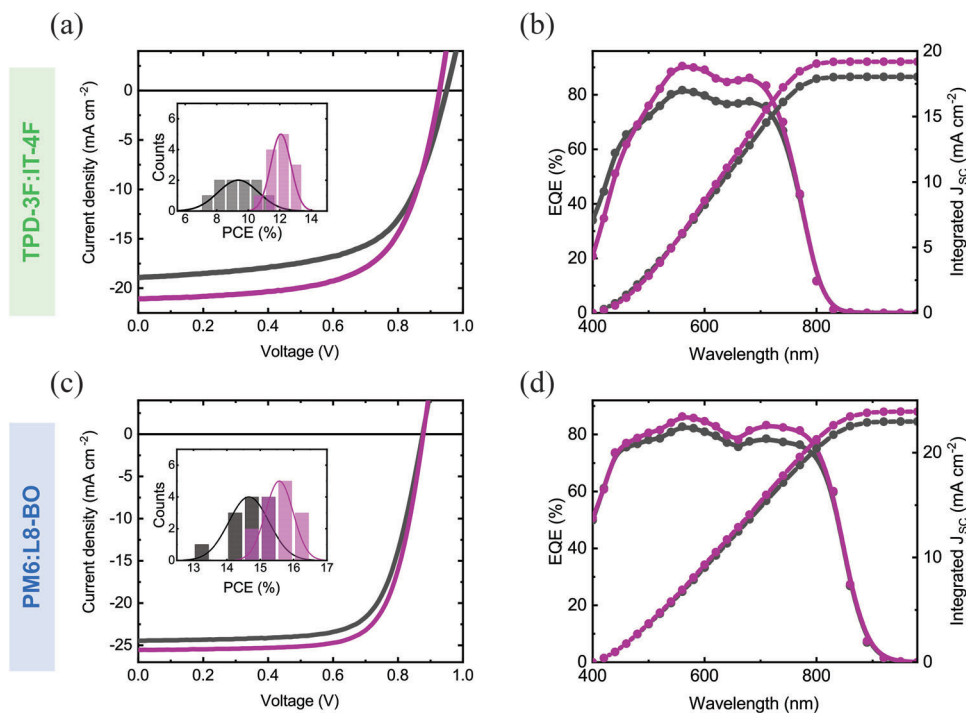


**Figure 3.** Electrical characterization and EQE of solar cells with pristine SnO<sub>2</sub> (black) and DI-washed SnO<sub>2</sub> (purple) conditions. *J*–*V* characteristics for solar cells fabricated with a) TPD-3F:IT-4F and c) PM6:L8-BO blends with the corresponding PCE histogram as figure inset; external quantum efficiency and integrated short-circuit current of the solar cells made with b) TPD-3F:IT-4F and d) PM6:L8-BO blends.

**Table 1.** Photovoltaic parameters of the record efficiency solar cells with pristine SnO<sub>2</sub> and SnO<sub>2</sub> washed with DI-water as active layers.

Active layer	SnO <sub>2</sub>	V <sub>OC</sub> [V]	J <sub>SC</sub> [mA cm <sup>-2</sup> ]	FF [%]	PCE <sub>max</sub> (PCE <sub>ave</sub> ) <sup>a)</sup> [%]
TPD-3F:IT-4F	Pristine	0.950	19.10	62	11.06 (9.37 ± 1.29)
	DI-washed	0.934	21.85	63	12.82 (12.07 ± 0.64)
PM6:L8-BO	Pristine	0.876	24.45	71	15.17 (14.66 ± 0.60)
	DI-washed	0.878	25.55	72	16.26 (15.57 ± 0.42)

<sup>a)</sup> Average and standard deviation values obtained from 12 distinct devices.

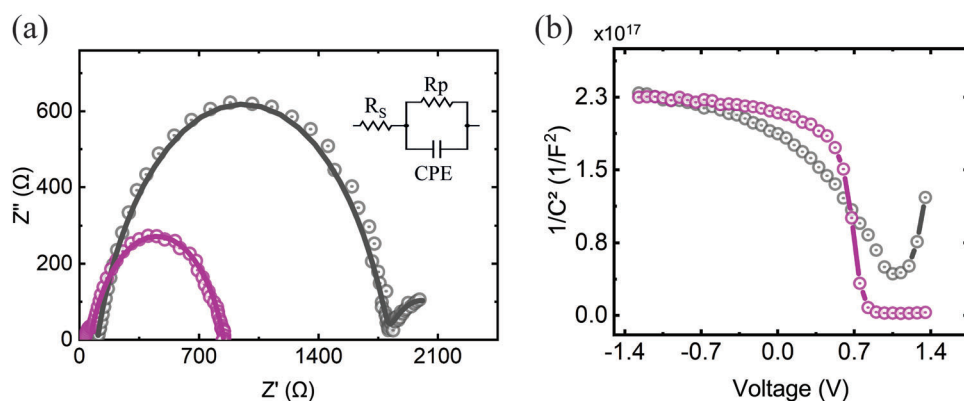


**Figure 4.** Impedance spectroscopy measurements. a) Nyquist plot of devices with pristine SnO<sub>2</sub> (black) and SnO<sub>2</sub> washed with DI water (purple). Fits (continuous lines) and the equivalent circuit (inset) are displayed; b) Mott–Schottky curves for both device conditions.

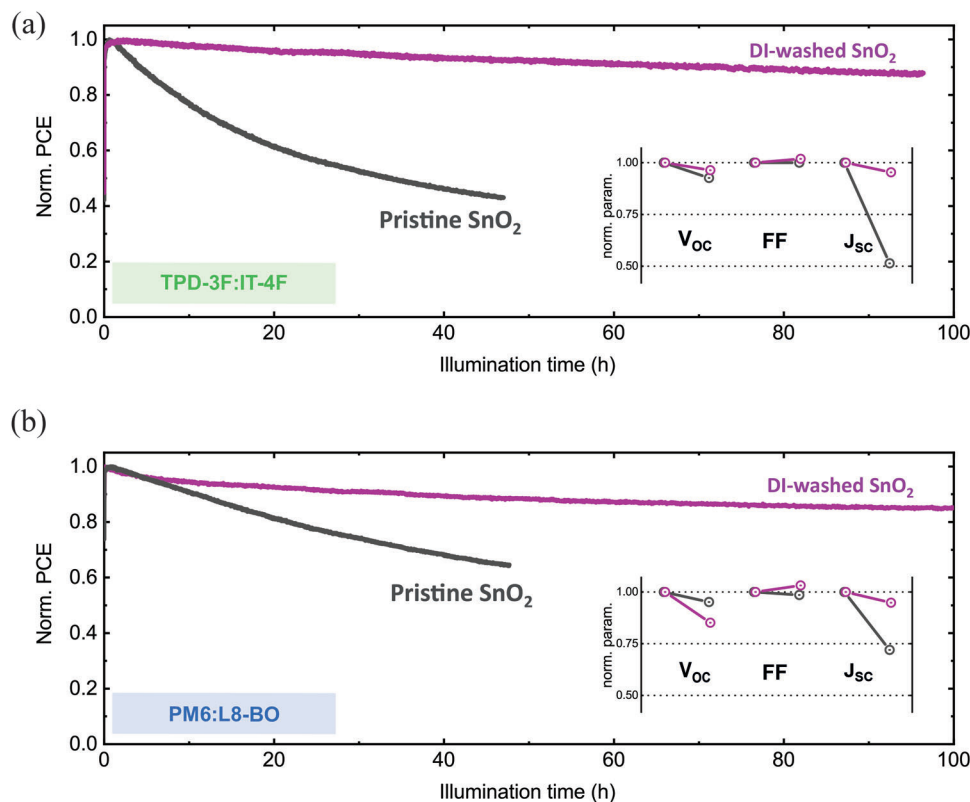


**Figure 5.** Stability under continuous illumination of the solar cells made with pristine SnO<sub>2</sub> and with SnO<sub>2</sub> washed with DI water. Normalized PCE over illumination time, and initial and final photovoltaic parameters for devices fabricated with a) TPD-3F:IT-4F and b) PM6:L8-BO blends.

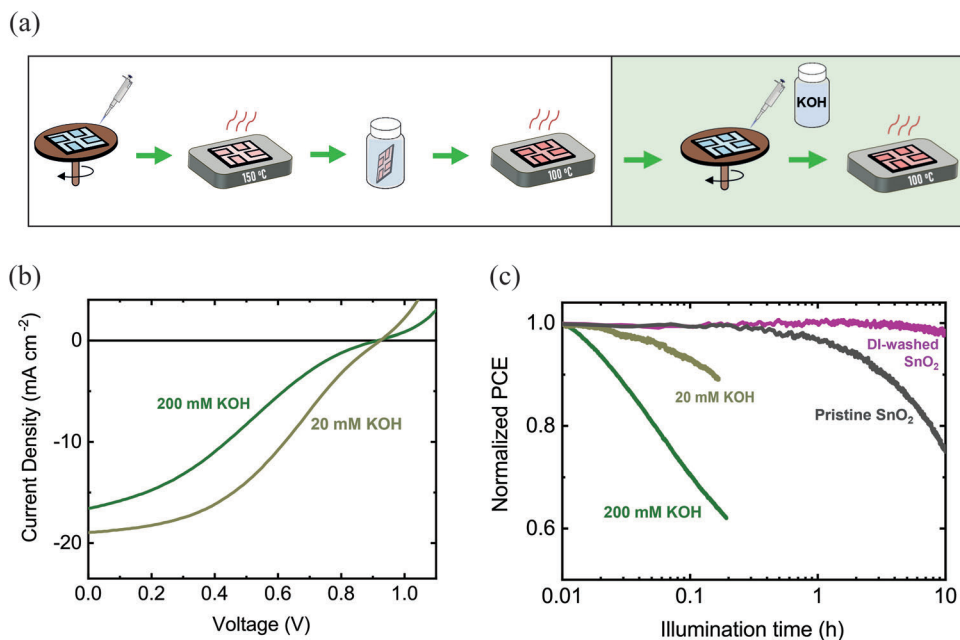
low frequencies ( $RC = 0.32$  s) for the pristine sample but not after washing. Ion motion occurs in this frequency range, so we speculate that potassium ions are released from the surface and are electrically coupled with the AC bias, therefore contributing to another capacitive element.<sup>[36]</sup>

Figure 4b displays the Mott–Schottky curve measured for both device types. At high negative bias, the geometric capacitance dominates and is almost uniquely influenced by the dielectric constant and layer thickness.<sup>[37]</sup> The overlap of the capacitance values under these conditions suggests that washing had no effect on the bulk properties, and further proves the electrical differences strictly originate from the interface modification. For positive applied bias, the capacitance increased due to the modulation of the depletion region, and the slope of the Mott–Schottky curve ( $C^{-2}$  vs applied voltage) is determined by the apparent doping density ( $N_A$ ).<sup>[38]</sup> While in highly doped systems this value depends on the doping density, in low-doped organic systems it is dominated by the injected charge carriers, which give rise to a chemical capacitance. This contribution is strongly correlated with the excess of charges accumulated at the interface.<sup>[37,38]</sup> The  $N_A$  dropped from  $1.3 \times 10^{16} \text{ cm}^{-3}$  to  $2.3 \times 10^{15}$  with the SnO<sub>2</sub> washing, demonstrating that the removal of potassium promoted a lower charge accumulation at the interface.

To further investigate the influence of the surface ions on the charge extraction mechanism, the surface potential of the SnO<sub>2</sub> films before and after the wash was measured by Kelvin probe force microscopy. The fermi level downshifts from  $-4.29$

to  $-4.48$  eV with the water wash. The charge unbalance present on the surface of the pristine SnO<sub>2</sub> would generate an interfacial dipole producing band bending at the interface, and increasing the fermi-level pinning with the interfacial states (Figure S6, Supporting Information). The filling of these states over time of illumination may alleviate the fermi-level pinning, reducing the s-shaped observed above. On the contrary, when the surface ions are removed with the DI-wash, the reduction of the dipole downshifts the fermi level, and the fermi-level pinning is removed. As a consequence, we reduce charge accumulation and eliminate the s-shape. This is in agreement with the observed reduction in surface recombination with impedance spectroscopy and points out the increase in charge extraction as responsible for the improved performance.

Besides the performance, device stability can be strongly affected by the interface properties.<sup>[39]</sup> Figure 5 displays the maximum power point (MPP) tracking of the solar cells fabricated with pristine SnO<sub>2</sub> and with DI-washed SnO<sub>2</sub> under continuous illumination, together with the initial and final photovoltaic parameters. Poor device lifetimes of  $\approx 40\%$  and  $\approx 60\%$  of their initial PCEs after 50 h of continuous illumination were observed using pristine NPs with TPD-3F:IT-4F and PM6:L8-BO, respectively. Such rapid degradation further justifies the need for surface passivation reported in the literature for devices where this type of nanoparticles was used.<sup>[19,23]</sup> Following the removal of the potassium ions by washing, the lifetime of the solar cells with both blends was enhanced, showing up to  $\approx 87\%$  and  $\approx 85\%$  of their initial PCEs after 100 h of



**Figure 6.** Fabrication of solar cells where the  $\text{SnO}_2$  film was first washed with DI water and then exposed to KOH in water. a) Schematic of the KOH-treatment process; b)  $J$ - $V$  characteristics of the devices treated with KOH with concentrations of 20 and 200 mM; c) stability under light of the solar cells with the KOH-treated  $\text{SnO}_2$ , compared to that of devices fabricated with pristine and with washed  $\text{SnO}_2$ .

continuous illumination for TPD-3F:IT-4F and PM6:L8-BO, respectively. For the devices fabricated with pristine  $\text{SnO}_2$ , the most affected parameter was the short-circuit current, which dropped to 50.7% for the first blend and to 71.6% for the second one. In the case where  $\text{SnO}_2$  was washed, a minimal drop of  $\approx 5\%$  was observed after 100 h of continuous illumination for both blends. This shows that the presence of potassium not only limited the maximum current extraction of the freshly prepared devices but also induced interfacial degradation. Washing with DI water is an effective and easy way to systematically prevent these shortcomings without the need for complex passivation procedures.

Finally, to further confirm that the potassium cations at the interface are responsible for the low efficiency, the s-shaped  $J$ - $V$  characteristics, and the poor device lifetimes, we fabricated TPD-3F:IT-4F solar cells in which we employed KOH to add potassium to the  $\text{SnO}_2$  surface after washing with DI water (Figure 6a). XPS was again employed to verify that potassium from KOH bonds on the washed surface (see Figure S7, Supporting Information). Two concentrations of KOH in water were tested namely 20 and 200 mM. The device where the surface had been treated with 20 mM KOH in water showed a very pronounced s-shape of the  $J$ - $V$  curve. The device characteristics of the 200 mM KOH were even worse (Figure 6b). Therefore, we demonstrate that the potassium addition reestablished a defective interface, which constituted a stronger barrier for electron extraction. Additionally, in Figure 6c we compare the stability under illumination of devices fabricated with pristine and with washed  $\text{SnO}_2$ , with those where the washed  $\text{SnO}_2$  film was treated with KOH in water; again, we observed a correlation between the concentration of potassium and the device lifetime, corroborating our previous observations.

### 3. Conclusion

In conclusion, we have shown for the first time how the intrinsic challenges of a well-known and scalable  $\text{SnO}_2$  formulation employed in organic solar cells can be overcome with a simple wash with DI water. We demonstrated that residual potassium ions bound on the surface of  $\text{SnO}_2$ -casted films form a barrier for effective electron extraction in solar cells, leading to poor device performance and lifetimes. By just removing the ions through the washing, we improve the efficiencies to reach 12.82% for solar cells containing a TPD-3F:IT-4F blend and 16.26% for those made with PM6:L8-BO. Interestingly, the devices made with the washed films showed a substantial boost in the short-circuit current due to an improved charge extraction. Moreover, and most significantly, the operational stability was highly improved by potassium removal, leading the two tested systems to remarkable PCEs of  $\approx 87\%$  and  $\approx 85\%$  of their initial value after 100 h of continuous illumination. Finally, we demonstrated empirically that the bound ions are responsible for the defective interface, and that surface washing can be employed to improve the interface quality without further need for passivation. Overall, this work opens the path for low-cost  $\text{SnO}_2$  to be optimally used as an electron transport layer for efficient and stable organic solar cells.

### 4. Experimental Section

**Materials:** Tin oxide colloidal nanoparticles (colloidal dispersion 15 wt.% in water) were purchased from Alfa Aesar. TPD-3F and IT-4F were purchased from Raynergy Tek. PM6 and L8-BO were purchased from Solarmer Energy. *o*-Xylene (99%) was purchased from Acros Organics.



Chloroform ( $\geq 99\%$ ) and 1,8-diiodooctane (98%) were purchased from Sigma–Aldrich. All chemicals were used without any further purification.

**Solar Cell Fabrication:** Solar cells with an n-i-p structure ITO/ETL/active layer/MoO<sub>x</sub>/Al were fabricated on pre-patterned ITO glass substrates. For the TPD-3F:IT-4F blend, the solution was prepared with a polymer concentration of 9 mg mL<sup>-1</sup> (1:1) in *o*-Xylene and stirred at 120 °C for 12 h. For the PM6:L8-BO blend, the solution was prepared with a polymer concentration of 7.5 mg mL<sup>-1</sup> (1:1.2) in chloroform and stirred at 50 °C for 2 h, with 1,8-diiodooctane as an additive (0.25 vol%). A SnO<sub>2</sub> solution was prepared by diluting the precursor solution in water with a 1:2 ratio (SnO<sub>2</sub>:H<sub>2</sub>O). Substrates were cleaned with soapy water, deionized water, acetone, and isopropyl alcohol. Before the deposition of the electron transport layers, a UV/Ozone process was employed on the substrates for 20 min. SnO<sub>2</sub> layers were spin-coated on the substrates at 3000 RPM for 40 s, forming a  $\approx 25$  nm thick layer, followed by thermal annealing at 150 °C for 30 min. No treatment was performed on the pristine SnO<sub>2</sub> before the active layer was deposited. For the surface treatment, a separate group of thermally annealed SnO<sub>2</sub> films was immersed in a small beaker with deionized water for 1 min, and dried in air at 100 °C for 10 min. For the reserve experiment, a solution of KOH in water was spin-coated on top of the DI-washed SnO<sub>2</sub> films, followed by a thermal annealing of 100 °C for 10 min to remove the water residuals.

Blend films were deposited via spin coating in the N<sub>2</sub> atmosphere. For the TPD-3F:IT-4F blend, the deposition was done at 1500 rpm for 60 s with annealing at 120 °C for 10 min. The PM6:L8-BO blend was deposited at 3000 rpm for 30 s and thermal annealing was performed at 100 °C for 10 min. A MoO<sub>x</sub> layer of 10 nm and an Al layer of 100 nm was thermally evaporated to finish the devices at  $\approx 10^{-6}$  mbar

**SnO<sub>2</sub> Nanoparticles Characterization:** Zetasizer Ultra Malvern Instrument was used to measure DLS and zeta potential, which is equipped with a HeNe laser ( $\lambda = 632.8$  nm).

**Thin Film Characterization:** Atomic Force Microscopy (AFM) and Kelvin Probe Force Microscopy (KPFM): micrographs of the pristine and washed SnO<sub>2</sub> films were collected with a Bruker MultiMode-8 microscope equipped with ScanAsyst automatic image optimization, and the data were analyzed with Gwyddion data analysis software. KPFM measurements were performed on the same Bruker microscope, using SCM-PIT-V2 probes (resonant frequency 75 kHz, spring constant 3 N m<sup>-1</sup>) and the Electrical & Magnetic Lift Modes/Surface potential (FM-KPFM). A freshly cleaved highly ordered pyrolytic graphite with a WF of 4.6 eV was used to determine the WF of the tip.

**Ellipsometry:** A J. A. Woollam Co. UV–vis ellipsometer (M2000) was used, with the software WVase32 to collect and analyze the data. A sample with a known optical constant (27 nm of SiO<sub>2</sub> on a Si wafer) was used for the system calibration. The measurements were carried out at incident angles from 70° to 75° and the wavelength range of 300–1700 nm was covered. SnO<sub>2</sub> nanoparticle films were measured on top of silicon substrates with native oxide.

**Fourier Transform Infrared (FTIR) Spectroscopy:** Attenuated total reflectance (ATR) FTIR spectra of the SnO<sub>2</sub> films were acquired in the range of 400–4000 cm<sup>-1</sup> with a Shimadzu IRTracer-100 spectrometer, with an incidence angle of 45° and a ZnSe prism and equipped with a KBr beam splitter and deuterated L-alanine doped triglycine sulfate (DLATGS) detector. Each spectrum had an average of 50 scans.

**X-Ray Photoelectron Spectroscopy (XPS):** XPS measurements on the SnO<sub>2</sub> films were performed on an SSX-100 (Surface Science Instruments) photoelectron spectrometer, equipped with a monochromatic Al K<sub>α</sub> X-ray source ( $h\nu = 1486.6$  eV) and operating at a pressure of  $1 \times 10^{-9}$  mbar. The photoelectron take-off angle was 37° with respect to the surface normal. The analyzed spot size on the sample was 1000  $\mu$ m in diameter. The experimental resolution was set to 1.67 eV for the overview spectra and to 1.26 eV for the detailed scans of the various core-level regions. Binding energies (BEs) are reported with  $\pm 0.1$  eV accuracy and referenced to the C1s core level at 284.8 eV.<sup>[40]</sup> All XPS spectra were analyzed using the least-squares curve-fitting program Winspec (developed at LISE, University of Namur, Namur, Belgium). Fitting of the spectra included a Shirley background subtraction and fitting with a minimum

number of peaks consistent with the chemical structure of the sample, taking into account the experimental resolution. The profile of the peaks was taken as a convolution of Gaussian and Lorentzian functions. The uncertainty in the peak intensity determination is 2% for all core levels reported.

**Device Characterization:** *J*–*V* measurements were performed under a simulated AM 1.5 G spectrum with a Steuernagel solar constant 1200 metal halide lamp, in an inert atmosphere, and at a constant temperature of 295 K. The illuminated area was defined by a shadow mask of 0.04 cm<sup>2</sup>. The light intensity was calibrated with a monocrystalline silicon solar cell (WRVS reference cell, Fraunhofer ISE). The operational stability was measured on samples encapsulated with  $\approx 40$  nm of Al<sub>2</sub>O<sub>3</sub> deposited by ALD. The external quantum efficiency (EQE) was measured using a xenon lamp and a set of band-pass filters, giving a spectral range of 400–1400 nm. After being filtered, the light was directed through a chopper and focused on the devices. The photocurrent was measured with a lock-in amplifier (Stanford Research Systems SR830 DSP). For the photon flux calibration, two Newport optical power detectors (Newport 818-SL and 818-IR) were used. The solar cells were kept in a nitrogen atmosphere during the measurements. For the impedance spectroscopy measurements, a Solarton 1260 impedance gain-phase analyzer was used. The DC voltage was set to open circuit conditions and the AC voltage was set to 20 mV to ensure linearity. The solar cells were kept in a nitrogen atmosphere and dark during the measurements. The equivalent circuit was fitted using the software Zview.

## Supporting Information

Supporting Information is available from the Wiley Online Library or from the author.

## Acknowledgements

This is a publication by the Focus Group “Next Generation Organic Photovoltaics” participating with the Dutch Institute for Fundamental Energy Research (DIFFER), both of which are part of the research program of the Foundation for Nederlandse Wetenschappelijk Onderzoek Instituten (NWO-I), part of the Dutch Research Council (NWO). L.D.M. and M.A.L. acknowledge funding from SOLAR-ERA.NET (project No. NFA4R2ROPV). This project was carried out with a subsidy from the Ministry of Economic Affairs and Climate Policy, Top Sector Energy subsidy scheme implemented by the Netherlands Enterprise Agency and received additional support from the Advanced Materials research program of the Zernike Institute for Advanced Materials under the Bonus Incentive Scheme (BIS) of the Netherlands Ministry of Education, Science, and Culture. The authors thank F. Ferrari and T. Zaharia for their help with ellipsometry measurements. The authors thank T. Zaharia and A. Kamp for their technical support.

## Conflict of Interest

The authors declare no conflict of interest.

## Data Availability Statement

The data that support the findings of this study are available from the corresponding author upon reasonable request.

## Keywords

electron transport layer, organic solar cells, stability, tin oxide

Received: July 13, 2023  
Revised: September 20, 2023  
Published online:

- [1] L. Zhu, M. Zhang, J. Xu, C. Li, J. Yan, G. Zhou, W. Zhong, T. Hao, J. Song, X. Xue, Z. Zhou, R. Zeng, H. Zhu, C.-C. Chen, R. C. I. Mackenzie, Y. Zou, J. Nelson, Y. Zhang, Y. Sun, F. Liu, *Nat. Mater.* **2022**, *21*, 656.
- [2] C. Li, J. Zhou, J. Song, J. Xu, H. Zhang, X. Zhang, J. Guo, L. Zhu, D. Wei, G. Han, J. Min, Y. Zhang, Z. Xie, Y. Yi, H. Yan, F. Gao, F. Liu, Y. Sun, *Nat. Energy* **2021**, *6*, 605.
- [3] A. Armin, W. Li, O. J. Sandberg, Z. Xiao, L. Ding, J. Nelson, D. Neher, K. Vandewal, S. Shoaee, T. Wang, H. Ade, T. Heumüller, C. Brabec, P. Meredith, *Adv. Energy Mater.* **2021**, *11*, 3570.
- [4] C. Guo, D. Li, L. Wang, B. Du, Z.-X. Liu, Z. Shen, P. Wang, X. Zhang, J. Cai, S. Cheng, C. Yu, H. Wang, D. Liu, C.-Z. Li, T. Wang, *Adv. Energy Mater.* **2021**, *11*, 2000.
- [5] L. Ye, K. Weng, J. Xu, X. Du, S. Chandrabose, K. Chen, J. Zhou, G. Han, S. Tan, Z. Xie, Y. Yi, N. Li, F. Liu, J. M. Hodgkiss, C. J. Brabec, Y. Sun, *Nat. Commun.* **2020**, *11*, 6005.
- [6] X. Song, G. Liu, W. Gao, Y. Di, Y. Yang, F. Li, S. Zhou, J. Zhang, *Small* **2021**, *17*, 6387.
- [7] N. Sukharevska, D. Bederak, D. Dirin, M. Kovalenko, M. A. Loi, *Energy Technol.* **2020**, *8*, 0887.
- [8] X. Wen, S. Fang, Y. Xu, N. Zheng, L. Liu, Z. Xie, F. Würthner, *ACS Appl. Mater. Interfaces* **2019**, *11*, 34151.
- [9] Y. Jiang, L. Sun, F. Jiang, C. Xie, L. Hu, X. Dong, F. Qin, T. Liu, L. Hu, X. Jiang, Y. Zhou, *Mater. Horiz.* **2019**, *6*, 1438.
- [10] L. Di Mario, D. Garcia Romero, H. Wang, E. K. Tekelenburg, S. Meems, T. Zaharia, G. Portale, M. A. Loi, *Adv. Mater.* **2023**, *230*, 1404.
- [11] C. Altinkaya, E. Aydin, E. Ugur, F. H. Isikgor, A. S. Subbiah, M. De Bastiani, J. Liu, A. Babayigit, T. G. Allen, F. Laquai, A. Yildiz, S. De Wolf, *Adv. Mater.* **2021**, *33*, 5504.
- [12] G. K. Dalapati, H. Sharma, A. Guchhait, N. Chakraborty, P. Bamola, Q. Liu, G. Saianand, A. M. Sai Krishna, S. Mukhopadhyay, A. Dey, T. K. S. Wong, S. Zhuk, S. Ghosh, S. Chakraborty, C. Mahata, S. Biring, A. Kumar, C. S. Ribeiro, S. Ramakrishna, A. K. Chakraborty, S. Krishnamurthy, P. Sonar, M. Sharma, *J. Mater. Chem. A Mater.* **2021**, *9*, 16621.
- [13] C. Altinkaya, E. Aydin, E. Ugur, F. H. Isikgor, A. S. Subbiah, M. De Bastiani, J. Liu, A. Babayigit, T. G. Allen, F. Laquai, A. Yildiz, S. De Wolf, *Adv. Mater.* **2021**, *33*, 5504.
- [14] W. Ke, G. Fang, Q. Liu, L. Xiong, P. Qin, H. Tao, J. Wang, H. Lei, B. Li, J. Wan, G. Yang, Y. Yan, *J. Am. Chem. Soc.* **2015**, *137*, 6730.
- [15] G. K. Dalapati, H. Sharma, A. Guchhait, N. Chakraborty, P. Bamola, Q. Liu, G. Saianand, A. M. Sai Krishna, S. Mukhopadhyay, A. Dey, T. K. S. Wong, S. Zhuk, S. Ghosh, S. Chakraborty, C. Mahata, S. Biring, A. Kumar, C. S. Ribeiro, S. Ramakrishna, A. K. Chakraborty, S. Krishnamurthy, P. Sonar, M. Sharma, *J. Mater. Chem. A Mater.* **2021**, *9*, 16621.
- [16] Q. Jiang, L. Zhang, H. Wang, X. Yang, J. Meng, H. Liu, Z. Yin, J. Wu, X. Zhang, J. You, *Nat. Energy* **2017**, *2*, 177.
- [17] C. Altinkaya, E. Aydin, E. Ugur, F. H. Isikgor, A. S. Subbiah, M. De Bastiani, J. Liu, A. Babayigit, T. G. Allen, F. Laquai, A. Yildiz, S. De Wolf, *Adv. Mater.* **2021**, *33*, 5504.
- [18] L. Di Mario, D. Garcia Romero, M. J. Pieters, F. Eller, C. Zhu, G. Bongiovanni, E. M. Herzig, A. Mura, M. A. Loi, *J. Mater. Chem. A Mater.* **2023**, *11*, 2419.
- [19] R. Yu, X. Wei, G. Wu, T. Zhang, Y. Gong, B. Zhao, J. Hou, C. Yang, Z. Tan, *Energy Environ. Sci.* **2022**, *15*, 822.
- [20] S. Guang, J. Yu, H. Wang, X. Liu, S. Qu, R. Zhu, W. Tang, *J. Energy Chem.* **2021**, *56*, 496.
- [21] D. Yang, R. Yang, K. Wang, C. Wu, X. Zhu, J. Feng, X. Ren, G. Fang, S. Priya, S. Liu, S. (Frank) Liu, *Nat. Commun.* **2018**, *9*, 3239.
- [22] S. Huang, N. Ali, Z. Huai, J. Ren, Y. Sun, X. Zhao, G. Fu, W. Kong, S. Yang, *Org. Electron.* **2020**, *78*, 105555.
- [23] H. Gao, X. Wei, R. Yu, F.-Y. Cao, Y. Gong, Z. Ma, Y.-J. Cheng, C.-S. Hsu, Z. Tan, *Adv. Opt. Mater.* **2022**, *10*, 2031.
- [24] R. Peng, T. Yan, J. Chen, S. Yang, Z. Ge, M. Wang, *Adv. Electron. Mater.* **2020**, *6*, 1245.
- [25] F. Zhao, L. Deng, K. Wang, C. Han, Z. Liu, H. Yu, J. Li, B. Hu, *ACS Appl. Mater. Interfaces* **2020**, *12*, 5120.
- [26] D. Garcia Romero, L. Di Mario, G. Portale, M. A. Loi, *J. Mater. Chem. A Mater.* **2021**, *9*, 23783.
- [27] A. Sundqvist, O. J. Sandberg, M. Nyman, J.-H. Smätt, R. Österbacka, *Adv. Energy Mater.* **2016**, *6*, 2265.
- [28] J. Luke, L. Corrêa, J. Rodrigues, J. Martins, M. Daboczi, D. Bagnis, J.-S. Kim, *Adv. Energy Mater.* **2021**, *11*, 3405.
- [29] C. S. Kim, S. S. Lee, E. D. Gomez, J. B. Kim, Y.-L. Loo, *Appl. Phys. Lett.* **2009**, *94*, 9947.
- [30] Y. Xu, Y. Qin, S. Palchoudhury, Y. Bao, *Langmuir* **2011**, *27*, 8990.
- [31] L. Ehrl, Z. Jia, H. Wu, M. Lattuada, M. Soos, M. Morbidelli, *Langmuir* **2009**, *25*, 2696.
- [32] C. Piliago, L. Protesescu, S. Z. Bisri, M. V. Kovalenko, M. A. Loi, *Energy Environ. Sci.* **2013**, *6*, 3054.
- [33] Nonappa, O. Ikkala, *Adv. Funct. Mater.* **2018**, *28*, 4328.
- [34] E. Von Hauff, *J. Phys. Chem. C* **2019**, *123*, 11329.
- [35] L. Duan, H. Yi, C. Xu, M. B. Upama, M. A. Mahmud, D. Wang, F. H. Shabab, A. Uddin, *IEEE J. Photovolt.* **2018**, *8*, 1701.
- [36] E. Von Hauff, D. Klotz, *J. Mater. Chem. C Mater.* **2022**, *10*, 742.
- [37] E. Von Hauff, *J. Phys. Chem. C* **2019**, *123*, 11329.
- [38] T. Kirchartz, W. Gong, S. A. Hawks, T. Agostinelli, R. C. I. Mackenzie, Y. Yang, J. Nelson, *J. Phys. Chem. C* **2012**, *116*, 7672.
- [39] M. A. Dheyab, A. A. Aziz, M. S. Jameel, N. Oladzadabbasabadi, *Surf. Interfaces* **2022**, *28*, 1677.
- [40] J. F. Moulder, W. F. Stickle, P. E. ' Sobol, K. D. Bomben, in *Handbook of X-Ray Photoelectron Spectroscopy* (Ed: J. Chastain), Perkin Elmer Corporation, MN, USA **1992**.